IOP Publishing Journal of Optics
J. Opt. **26** (2024) 025401 (5pp) https://doi.org/10.1088/2040-8986/ad21e0

Simultaneous mapping of the magnetic field components using near-field microscopy

Juan M Merlo[1,*], Raphael J Ettinger-Finley[1], Madeleine Hoag Carhart[1], Florence Binny[1] and Lázaro Merlo-Ramírez[2]

[1] Physics and Astronomy Department, Vassar College, 124 Raymond Ave., Poughkeepsie, NY 12604, United States of America
[2] Instituto Tecnológico de Puebla, Av. del Tecnológico #420. Col. Maravillas, Puebla 72220, Pue., Mexico

E-mail: jmerloramirez@vassar.edu

Received 30 August 2023, revised 12 January 2024
Accepted for publication 23 January 2024
Published 1 February 2024

Abstract

In this work, we present a near-field scanning optical microscope capable of simultaneously mapping the $x-$, $y-$, and $z-$ components of the magnetic field generated by a set of magnetic coils in the kHz range. Using this device, we present two experiments: the observation of the well-known magnetic field of a circular coil and a resolution test. The observations achieved with our instrument are supported by numerically calculated simulations, which confirm the validity of our experimental results. In addition, our instrument is capable of imaging features of the order of 15 mm, representing a resolution of $\lambda/10000$. Our approach establishes an important avenue for the three-dimensional mapping of the electromagnetic field in any spectral range, using the correct configuration of the probe, and opens a new discussion on the resolution of scanning probe microscopes imaging more than one component of the studied field.

Keywords: near-field microscopy, three-dimensional magnetic field, magnetic field components, electromagnetic induction

1. Introduction

Near-field microscopy (NFM) is a mature research area about the study of light-matter interactions with resolutions that overcome the classical resolution limit [1–3]. This research area has allowed the discovery of exciting phenomena in the last decade, particularly in the realm of plasmonics and two-dimensional materials [4–6]. Interestingly, the light intensity detected in near-field microscope, while raster scanning the sample surface, can be approximated as the total electric field strength of the interactions at the near-field region [7]. In addition, some recent works have developed methods to generate three-dimensional maps of the electric field [8–12]. On the other hand, the magnetic fields, another inherent part of the electromagnetic field, have been largely overlooked in the study of near-field interactions, though some recent approaches have begun to explore this subject [13–18]. Among them, the use of modified apertured near-field probes, where a small gap was generated so the probe acts as a split ring resonator [15], the use of dielectric pyramidal probes coated with metal that act as resonant rings [14], and even by using nanoparticles [18]. However, these approaches relied on complicated detection schemes or near-field probe geometries [14, 15].

Though the existing approaches to detecting the magnetic field at the near-field region have all attained important achievements [14, 15], a reliable and straightforward means of mapping the components of such magnetic field is still missing. In this sense, we present a non-reported approach for the detection of each component of the magnetic field in the near-field region. We demonstrate that our instrument is able to reproduce well-known theoretical results of circular magnetic coils. We believe that our approach can be

* Author to whom any correspondence should be addressed.

extended to higher frequencies through appropriate modifications in the sensing probe. We also provide evidence of the maximum resolution our instrument can reach, even reproducing results already reported in the NFM research [4, 5, 7] and expanding the knowledge of near-field probes resolution.

2. Instrumentation

2.1. Detection of the magnetic field components

In order to measure the three components of an oscillating magnetic field under analysis (MF-UA), we constructed a three-dimensional magnetic probe (3D-MP) using three orthogonal inductors (one per magnetic field component) with inductance of $L = 22\,\mu\text{H} \pm 2.2\,\mu\text{H}$, length $l = 2.4\,\text{mm} \pm 0.1\,\text{mm}$, and diameter $d = 5\,\text{mm} \pm 0.1\,\text{mm}$. Figure 1 shows a schematic representation of the 3D-MP where the direction of each component is set and the dimensions of the inductors. Due to the orthogonality of the inductors composing the 3D-MP, the electromagnetic induction between them was negligible with respect to the MF-UA. This characteristic allows us to treat the 3D-MP as a passive element with minimal effect on the MF-UA, as in the case of already reported NFM works [5, 7].

The operation principle of the 3D-MP can be described as follows: when the 3D-MP flew over the device generating the MF-UA, each inductor generated a current in response to the change in their magnetic flux in an independent way. The current was determined by the magnetic field as $i = BA/L$, where B is the magnetic field strength, and L and A are the inductance and transverse area of the inductor, respectively. Thus, the detection of such currents at each point over the sample surface generated a map of each component of the magnetic field.

Due to the linear relationship between the current and the magnetic field strength in each inductor, it was possible to measure such a current using a lock-in amplifier (LIA). The use of a LIA has four primary motivations; the first being to filter the signal generated by the inductors, suppressing the electromagnetic noise in the environment. The second reason was to amplify the magnitude of the signals generated by the inductors. The third reason was that the LIA excited the MF-UA with periodic signal used as reference. Finally, this method allowed us to measure both the strength and phase of the MF-UA and consequently determine its magnetic field components. This technique aligns with standard practice for scattering-based NFM [19].

2.2. The samples

Although our instrument was not limited to a specific kind of sample, for the purpose of the proof-of-concept, we used circular coils in two separate cases. In the first case, the coil was composed of 4 turns of wire in a flat configuration. The inner and outer diameters of the coil were $30.0\,\text{mm} \pm 0.1\,\text{mm}$ and $40.0\,\text{mm} \pm 0.1\,\text{mm}$, respectively, and thickness was $2\,\text{mm} \pm 0.1\,\text{mm}$. In the second case, we used a set of circular coils composed of 20 turns with diameters of $15.0\,\text{mm} \pm 0.2\,\text{mm}$ and heights of $1.0\,\text{mm} \pm 0.2\,\text{mm}$.

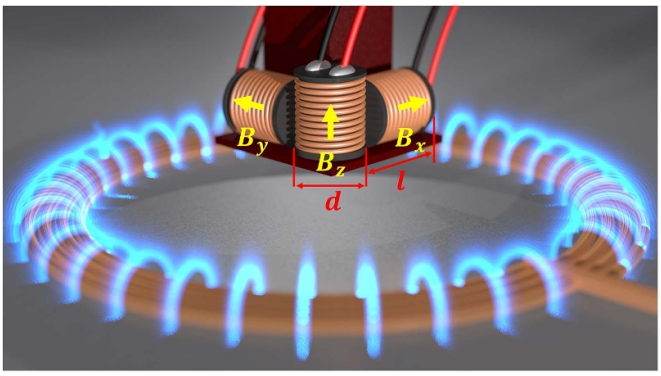

Figure 1. Schematic representation of the three-dimensional magnetic probe.

2.3. The scanner

The 3D-MP was mounted in a mechanical stage able to raster scan the sample at a fixed vertical distance. The maximum spatial resolution of the scanning stage was 50 μm, however, we decided to use a step size at a minimum of 200 μm to keep the uncertainty in the displacement small enough to avoid hysteresis effects affecting the overall performance of the instrument.

3. Results

Before describing our experimental results, it is important to note that all the results presented in this work were obtained by using an excitation signal with amplitude of 5 V and a frequency of 500 kHz, equivalent to a wavelength $\lambda = 600\,\text{m}$. This means that all the dimensions of our experiments were smaller than $\lambda/10\,000$, see sections 2.2 and 2.3, well beyond the classical diffraction limit [20], as mentioned before. The experimental impedance of the inductors composing the 3D-MP was measured to be 62.1 Ω at the excitation frequency.

3.1. Calibration

In our first experiment, as mentioned before, we used the circular coil with diameter of $40\,\text{mm} \pm 0.1\,\text{mm}$. Since the magnetic field generated by a circular coil is well-known, we chose to use this configuration to simplify the interpretation of the obtained images. The scanning was performed over an area of $100 \times 100\,\text{mm}^2$ at a fixed height of $5\,\text{mm} \pm 0.5\,\text{mm}$. Figures 2(a)–(c) shows the experimental data of the three components of the MF-UA. The dashed lines represent the actual position of the circular coil in each case. The dipole nature of the $x-$ and $y-$components and the monopole contribution of the $z-$ components are both clearly measured, as expected [21].

In order to confirm our experimental results, we performed numerical simulations using the finite element method. In this

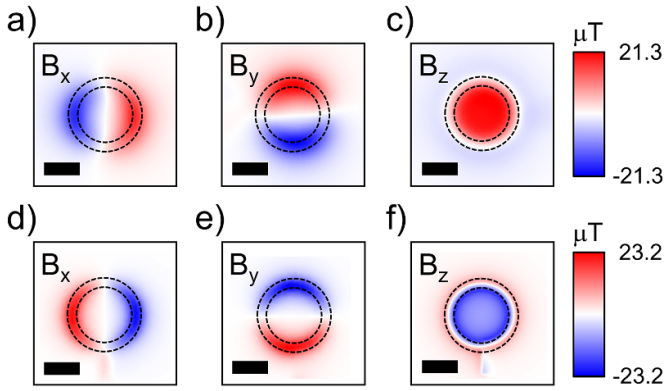

Figure 2. Comparison between experimental, (a), (b), and (c), and calculated magnetic field components, (d), (e), and (f). In all cases, the scale bar represents 20 mm. The $x-$ and $y-$ components were scaled up by a factor of two for better comparison.

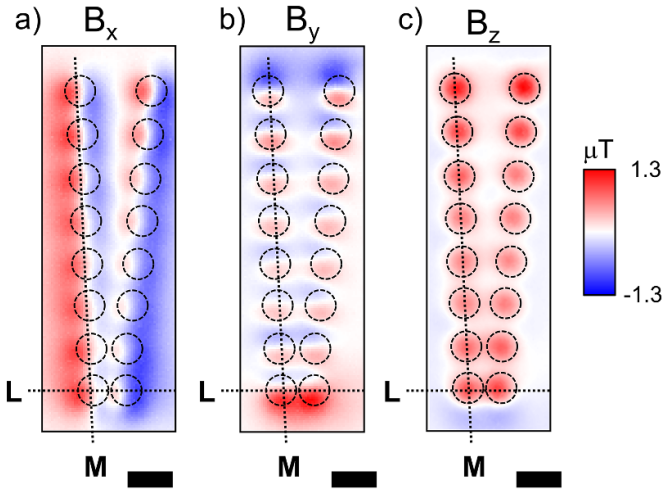

Figure 3. Resolution determination of each magnetic field component using experimental data. The scale bar represents 20 mm. Lines ***L*** and ***M*** were used for transverse cuts for resolution analysis. The $x-$ and $y-$ components were scaled up by a factor of two for better comparison.

case, a symmetry and dimensions similar to the circular coil were used. We assumed that the wire composing the coil was a perfect electric conductor. We emulated an excitation voltage of 5 *V* through a lumped port with current flowing in the same direction as the experimental case. Figures 2(d)–(f) summarizes the numerically calculated results. As in previous cases, the dashed lines represent the position of the circular coil.

It is clear by comparing the magnetic field components shown in figure 2 that the experimental results are consistent with the numerical calculations. Although our experimental and numerical results were similar, we found some important differences. Among these differences, we found that the magnetic field components in the experimental data, figures 2(a)–(c), are not strongly confined to the width of the circular coil, as they are in the case of the calculated field components, figures 2(d)–(f). We believe this is due to two factors: the finite size of the individual probes and the finite conductivity of the wire composing the coil under study.

Another interesting finding was that the experimental components have inverted phase with respect to the calculated ones. This happened because the experimentally measured currents in the 3D-MP were the response to the MF-UA, meaning that in order to preserve the magnetic flux, the inductors composing the 3D-MP responded with an inverted current with respect to the excitation current in the coil under study. Interestingly, the amplitude of the experimental and calculated magnetic field components were similar. This is due to the linear amplification of the current measured by the LIA.

3.2. Resolution

When a new microscopy configuration is proposed, one of the most important factors to be determined is the resolution. To calculate the resolution of our device, we measured the magnetic field components of a set of circular coils, each made of 20 turns of copper wire 1 mm diameter and 1 mm $\pm$ 0.1 mm height, as mentioned before. The diameter of the coils was 15.0 mm $\pm$ 0.2 mm, located at controlled center-to-center distances, ranging from 15 mm $\pm$ 0.5 mm to 35 mm $\pm$ 0.5 mm in steps of 5 mm $\pm$ 0.2 mm, in the $x-$ direction and fixed distances of 20 mm $\pm$ 0.2 mm in the $y-$ direction. Figure 3 shows the results of the resolution analysis, where the dashed lines represent the position of the coils. It is important to note that in all the coils, the current direction was the same.

Our resolution analysis was based on the Rayleigh criterion [20]. According to this criterion, the distance between the average intensity of two maxima and the minimum between them must be at least 20 % to consider such a distance resolved [20]. For this purpose, we extracted cross sections along lines ***L*** and ***M*** in figure 3 and calculated the magnitude of each component; the results are shown in figure 4. We selected line ***L*** to determine if the field component was resolved along the $x-$ direction. As it is clear from figure 4(a), the only resolved component was the $z-$ component, whereas the $x-$ and $y-$ components were not, see inset in figure 4(a). Line ***M*** was selected to test the resolution in the $y-$ direction. Unlike the ***L*** cut, it is clear that all the components were resolved along ***M***, see inset in figure 4(b).

In order to understand our experimental results in terms of resolution, we calculated numerically the magnetic field generated by an inductor with similar characteristics as the ones used in the 3D-MP. From our numerical results, see figure 5, we concluded that the distances at which the inductor could sense the MF-UA is about four times their length. This means that the resolution is impacted by not only the length of the inductors in the $x-$ and $y-$ components, but also by their ability to detect magnetic fields well beyond their axial dimensions. The case of the $z-$ component was different as such a component was detected at fixed distance, resulting in a measurement confined to the diameter of the inductor.

Our findings confirm a very well-known fact in scanning probe microscopes, i.e. the size of the probe determines the instrument resolution in the $z-$ direction [4]. Furthermore, our

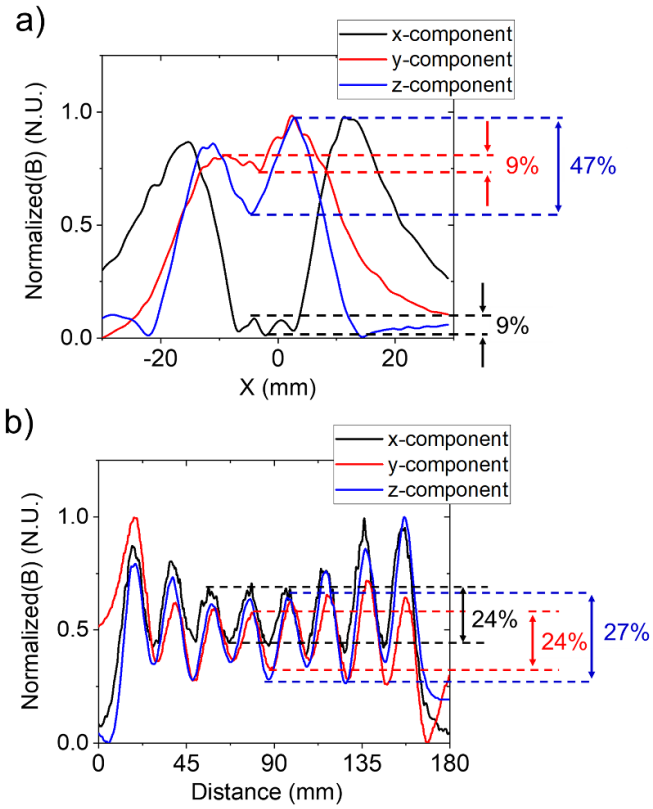

Figure 4. Resolution determination of each magnetic field component using the transverse cuts ***L*** (a) and ***M*** (b) of figure 3. In both cases, the magnitude of the magnetic field was used.

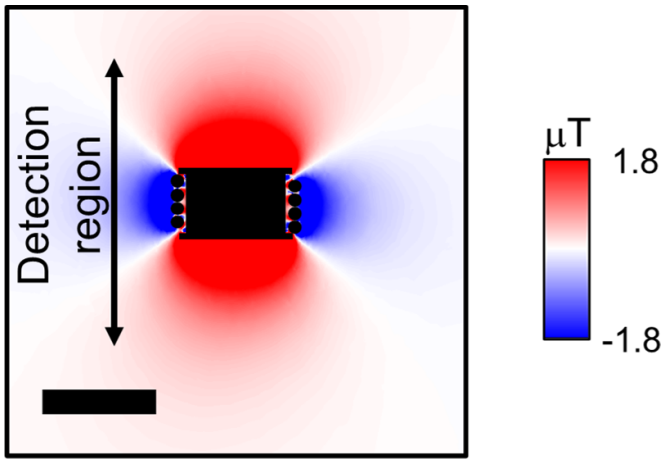

Figure 5. (a) Calculated magnetic field around an inductor with similar characteristics to the ones used in the 3D-MP. The scale bar represents 5 mm.

results extend this principle to the $x-$ and $y-$ components by determining the detection distance, as shown in figure 5. We believe these results could become the general case; however, this is a work in progress.

4. Discussion and conclusions

Although our method is a novel approach for the three-dimensional mapping of magnetic fields in the near-field, it is important to note that this experimental method is limited to frequencies below 100 MHz. The increase in impedance at higher frequency makes the inductors used in the 3D-MP insufficient. A set of split ring resonators [22] should enable measurements at higher frequencies, including optical ranges, so long as the perpendicular arrangement of the probe is retained. In the case of optical frequencies, it would be advised to use plasmonic metals to exploit their properties as optical antennas [7].

We have shown the implementation of a new configuration of a near-field microscope with the capability of measuring the three components of the magnetic field. It has been demonstrated that the measured magnetic components corresponded to the well-known theory in the case of a circular coil. An important finding was that the resolution of the instrument is dependent on the measured direction due to the finite size of the magnetic probe components. Our results complement the well-known resolution criterion in scanning probe microscopes, i.e. the size of the probe determines the minimum feature size to be resolved in the $z-$ component, while the $x-$ and $y-$ components are determined by the ability of the probe to sense the field beyond its axial dimensions. Our instrument opens the possibility for the three-dimensional mapping of the electromagnetic field in the near-field, not only in the kHz range, but also potentially extended to higher frequencies with the appropriate modifications in the structure of the magnetic probe and the materials used for its construction.

Data availability statement

All data that support the findings of this study are included within the article (and any supplementary files).

Acknowledgments

Juan M Merlo acknowledges Vassar College for startup funding number ST000057 and the URSI program 2022.

Authors' contributions

J M M conceived the Project; J M M and R E F performed the experiments; all authors contributed to the discussion, interpretation of the results, and wrote the manuscript.

Funding

There is no funding related to this work.

ORCID iD

Juan M Merlo https://orcid.org/0000-0002-3956-0940

References

[1] Harootunian A, Betzig E, Isaacson M and Lewis A 1986 Super-resolution fluorescence near-field scanning optical microscopy *Appl. Phys. Lett.* **49** 674–6

[2] Betzig E, Lewis A, Harootunian A, Isaacson M and Kratschmer E 1986 Near field scanning optical microscopy (NSOM) *Biophys. J.* **49** 269–79

[3] Ahs A and Nicholls G 1972 Super-resolution aperture scanning microscope *Nature* **237** 510–2

[4] Merlo J M, Ye F, Rizal B, Burns M J and Naughton M J 2014 Near-field observation of light propagation in nanocoax waveguides *Opt. Express* **22** 14148

[5] Nesbitt N T, Merlo J M, Rose A H, Calm Y M, Kempa K, Burns M J and Naughton M J 2015 Aluminum nanowire arrays via directed assembly *Nano Lett.* **15** 7294–9

[6] Kwon S, Kim J M, Ma P J, Guan W and Nam S 2023 Near-field nano-optical imaging of van der Waals materials *Adv. Phys. Res.* **2** 2300009

[7] Merlo J M, Nesbitt N T, Calm Y M, Rose A H, D'Imperio L, Yang C, Naughton J R, Burns M J, Kempa K and Naughton M J 2016 Wireless communication system via nanoscale plasmonic antennas *Sci. Rep.* **6** 31710

[8] Bazylewski P, Ezugwu S and Fanchini G 2017 A review of three-dimensional scanning near-field optical microscopy (3d-SNOM) and its applications in nanoscale light management *Appl. Sci.* **7** 973

[9] Dregely D, Neubrech F, Duan H, Vogelgesang R and Giessen H 2013 Vibrational near-field mapping of planar and buried three-dimensional plasmonic nanostructures *Nat. Commun.* **4** 2237

[10] Li Y, Zhou N, Raman A and Xu X 2015 Three-dimensional mapping of optical near field with scattering SNOM *Opt. Express* **23** 18730

[11] Rotenberg N and Kuipers L 2014 Mapping nanoscale light fields *Nat. Photon.* **8** 919–26

[12] Le Feber B, Sipe J E, Wulf M, Kuipers L and Rotenberg N 2019 A full vectorial mapping of nanophotonic light fields *Nat. Photon.* **8** 28

[13] Caselli N, Wu T, Arregui G, Granchi N, Intonti F, Lalanne P and Gurioli M 2021 Near-field imaging of magnetic complex mode volume *ACS Photonics* **8** 1258–63

[14] Denkova D, Verellen N, Silhanek A V, Valev V K, Dorpe P V and Moshchalkov V V 2013 Mapping magnetic near-field distributions of plasmonic nanoantennas *ACS Nano* **7** 3168–76

[15] Burresi M, Oosten D V, Kampfrath T, Schoenmaker H, Heideman R, Leinse A and Kuipers L 2009 Probing the magnetic field of light at optical frequencies *Science* **326** 550–3

[16] Kihm H W, Kim J, Koo S, Ahn J, Ahn K, Lee K, Park N and Kim D S 2013 Optical magnetic field mapping using a subwavelength aperture *Opt. Express* **21** 5625

[17] Vignolini S, Intonti F, Riboli F, Balet L, Li L H, Francardi M, Gerardino A, Fiore A, Wiersma D S and Gurioli M 2010 Magnetic imaging in photonic crystal microcavities *Phys. Rev. Lett.* **105** 123902

[18] Li G C, Xiang J, Zhang Y L, Deng F, Panmai M, Zhuang W, Lan S and Lei D 2021 Mapping the magnetic field intensity of light with the nonlinear optical emission of a silicon nanoparticle *Nano Lett.* **21** 2453–60

[19] Yang H U, Olmon R L, Deryckx K S, Xu X G, Bechtel H A, Xu Y, Lail B A and Raschke M B 2014 Accessing the optical magnetic near-field through Babinet's principle *ACS Photonics* **1** 894–9

[20] Calm Y M, Merlo J M, Burns M J and Naughton M J 2017 From airy to abbe: quantifying the effects of wide-angle focusing for scalar spherical waves *J. Opt.* **19** 105608

[21] Griffiths D J 1989 *Introduction to Electrodynamics* 2nd edn (Prentice Hall)

[22] Baena J D *et al* 2005 Equivalent-circuit models for split-ring resonators and complementary split-ring resonators coupled to planar transmission lines *IEEE Trans. Microw. Theory Tech.* **53** 1451